

Polarized neutron imaging at the CONRAD instrument at Helmholtz Centre Berlin

Ingo Manke^{1,2,*}, Nikolay Kardjilov¹, André Hilger¹, Markus Strobl^{1,3}, Martin Dawson¹, John Banhart^{1,2}

¹ Helmholtz Centre Berlin for Materials and Energy, 14109 Berlin, Germany

² Berlin Institute of Technology, 10623 Berlin, Germany

³ Ruprecht Karls University Heidelberg, 69120 Heidelberg, Germany

Keywords: magnetic imaging, neutrons, radiography, skin effect,

Abstract

Neutrons are highly sensitive to magnetic fields because of their intrinsic magnetic moment. At the same time their zero net electrical charge allows them to penetrate thick layers of matter. In combination with standard radiographic and tomographic imaging techniques these properties have been exploited to visualize magnetic fields in free space and within the bulk of solid, massive, opaque samples. In this paper, the basic principle of this new technique and its realization at the CONRAD instrument at the Helmholtz Centre Berlin (formerly Hahn-Meitner Institute Berlin) are explained. Two application examples will be given: the visualization of the magnetic field around a permanent magnet and the investigation of the displacement of the current density from the core of a conductor to the surface (the skin effect).

* Corresponding author. Tel.: +493080622682; fax: +493080623059. E-mail address: manke@helmholtz-berlin.de.

1. Introduction

Conventional approaches for imaging magnetic fields are limited to investigating the surface of a sample and the free space around it. Experimental methods such as scanning SQUID, Kerr effect, magnetic force, Faraday rotation or Lorentz (electron) microscopy, to name just a few, provide only limited access to information about the magnetic field distribution inside the bulk of a sample [1,2]. Neutrons on the other hand are particles that do not carry an electric charge and interact mainly with the nucleus of an atom [3,4]. This enables them to penetrate thicker layers of matter and makes them sensitive to distinguish isotopes [5-10]. In addition, neutrons carry a magnetic moment and can thus interact with magnetic fields. Both properties make neutrons a unique probe for the investigation of magnetic fields in the bulk of materials. Therefore neutron scattering methods such as diffraction, reflectometry, or small-angle scattering are indispensable tools in magnetism research.

Recently the magnetic sensitivity of neutrons has been exploited for standard neutron radiography and tomography. This allows the visualization of the two- and three-dimensional distribution of magnetic fields in free

space and in the bulk of materials [11-14].

2. Polarized neutron imaging

The neutron's magnetic moment, $\vec{\mu}$ ($-9.66 \times 10^{-27} \text{ J}\cdot\text{T}^1$) is aligned anti-parallel to its associated spin. An externally applied magnetic field, \vec{B} , causes a precession of the spin vector, \vec{S} , that can be described by the equation of motion (Fig. 1)

$$\frac{d}{dt} \vec{S} = \gamma [\vec{S}(t) \times \vec{B}(t)]$$

where γ is the gyromagnetic ratio of the neutron ($-1.832 \times 10^{-8} \text{ rad}\cdot\text{s}^{-1}\cdot\text{T}^1$) and

$$\gamma = \frac{g\mu_N}{\hbar}$$

where μ_N is the nuclear magneton, $g = -3.826$ is the g-factor and \hbar is the Dirac constant ($1.0546 \times 10^{-34} \text{ J}\cdot\text{s}$). It can be shown that the polarisation of an ensemble of neutrons behaves exactly like a classical magnetic moment [15]. The precession of the spin component perpendicular to the applied magnetic field will undergo a Larmor rotation with a frequency ω (Fig. 1), given by

$$\omega = \gamma B$$

where B is the norm of the magnetic field strength $B = |\vec{B}|$. For a neutron travelling along a path, s , with a velocity, v , the total precession angle, φ , is

$$\varphi = \frac{\gamma}{v} \int B ds = \frac{\gamma \lambda m}{2\pi\hbar} \int B ds \quad (\text{eq. 1})$$

where λ is the neutron wavelength and m is the neutron rest mass (1.675×10^{-27} kg). The transmitted signal of the spin analyzer depends on the spin rotation angle φ (eq. 1) and has a maximum for parallel ($2n\pi$) and a minimum for anti-parallel ($(2n+1)\pi$) spin orientation with respect to the analyzer.

φ is dependent on the neutron wavelength. Thus for precise quantification of the data a monochromatic beam is desirable. A polychromatic beam would dephase upon precession, resulting in a loss of polarisation. This is schematically explained in Figure 2. Depending on the amount of 2π rotations the (mean) neutron spin undergoes the higher is dephasing.

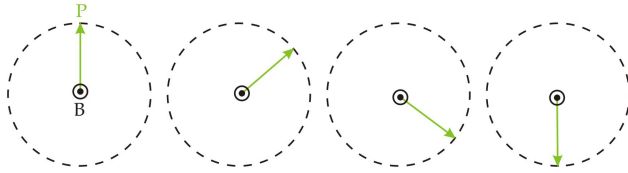


Figure 1: The orientation of the neutron's polarization axis will precess, if there is a significant perpendicular magnetic field component.

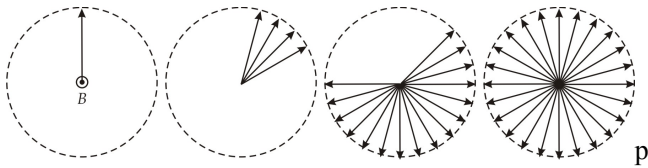


Fig. 2: Dephasing of a polychromatic neutron beam: Precession will cause a polychromatic neutron beam to dephase and depolarise in the plane perpendicular to the field.

The principle of polarized neutron imaging is described in Fig. 3. A neutron beam is spin-polarized, the neutrons traverse the magnetic field of the sample and the resulting spin is then analyzed with spatial resolution.

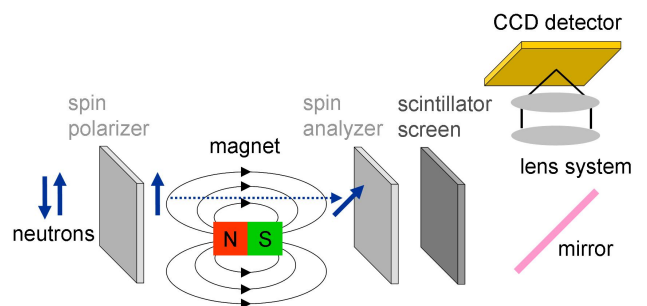


Fig. 3: A schematic diagram of the experimental setup used for polarised neutron imaging on CONRAD.

The transmission signal behind the spin analyzer at a location (x,y) in the detector plane is given by

$$I(x,y) = I_0(x,y) \cdot \exp\left(-\int_{\text{path}} \Sigma(s) ds\right) \cdot \frac{1}{2} \left(1 + \cos \varphi(x,y)\right) \frac{I_a(x,y)/I_0(x,y)}{I_m(x,y)/I_0(x,y)}$$

where $\varphi(x,y)$ is the position dependant angle between the analyzer orientation (which is parallel to the initial polarisation direction) and the magnetic moment of the neutron, $I_0(x,y)$ is the initial beam intensity, $\Sigma(s)$ is the linear attenuation coefficient of the sample along the path s . $I_a(x,y)$ represents the conventional attenuation contrast and $I_m(x,y)$ the contrast variations due to spin rotation.

Thus, for monochromatic neutrons, the measured intensity correlates directly to the cumulated precession angle and so to the average strength of the magnetic field through which the neutrons passed (see eq. 1).

In simple cases, the magnetic field to be visualized in and around a sample is comparably weak (about 0.1-10 mT) and aligned perpendicular to the (initial) neutron spin polarization direction, such that the overall rotation of the neutron spin is not more than π .

3. Experimental Setup

The experiments were carried out at the COLD Neutron RADiography facility CONRAD at the BER II reactor of the Helmholtz Centre Berlin (formerly Hahn-Meitner Institute Berlin). This instrument is placed at the curved neutron guide NL1b. A monochromatic beam with a wavelength of 0.33 nm was chosen for all experiments. The double-crystal monochromator used (pyrolithic graphite crystals with a mosaic spread of 3.5°) provided a wavelength resolution of $\Delta\lambda/\lambda \approx 12\%$ (full width half maximum) and a flux density of the order of $10^5 \text{ cm}^{-2}\text{s}^{-1}$. An ANDOR DW436N-BV CCD camera was used in conjunction with a 0.2 mm NDG scintillating screen to detect the neutrons. The spatial resolution of the recorded images was found to be below 500 μm for the given experimental geometry [5, 11].

Solid state polarizing benders constructed from a stack of

100 bent single-crystal silicon wafers were used [16]. They provide a beam with a cross-section of width \times height = 15 mm \times 45 mm and were applied for both polarisation and polarisation analysis. The typical polarisation achieved with such a bender is 95%. A cadmium screen with a window 1 \times 4 cm was placed in front of each bender. This prevents neutrons which had not passed through both benders from reaching the detector.

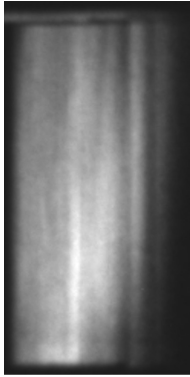


Fig. 4: A polarized neutron radiograph showing a flat field image (without sample) taken with solid state polarizing benders. Image size is about 24x50 mm².

Figure 4 shows a flat field radiograph (i.e. without sample) taken with this setup. The line structure is caused by the lamella of the solid state benders. In order to enable the investigation of samples larger than the beam and to eliminate the stripes the samples were scanned together with the detector through the beam defined by the fixed polarizing benders. Fig. 5 a) shows a flat field image taken with the scanning setup. For a single image on a scan path of 6 cm an exposure time of 15 minutes was necessary.

4. Experimental results

An example for this is shown in Fig 5 b) which displays a radiograph of a permanent magnet levitated above a superconductor ($\text{YBa}_2\text{Cu}_3\text{O}_7$ at 60 K) and illustrates the decay of the magnetic field strength with increasing distance from the magnet. This results in an annular structure around the sample with an increasing period due to the resulting precession angles of the neutron spin on their path through the strongly decaying field; bright (dark) regions of the image indicate where the measured neutron spin is oriented parallel (anti-parallel) to the polarization of the analyzer. The structure in the central part cannot be seen due to the coarse spatial resolution of approximately 500 μm ; here the field is stronger and the ring structures are correspondingly closer together.

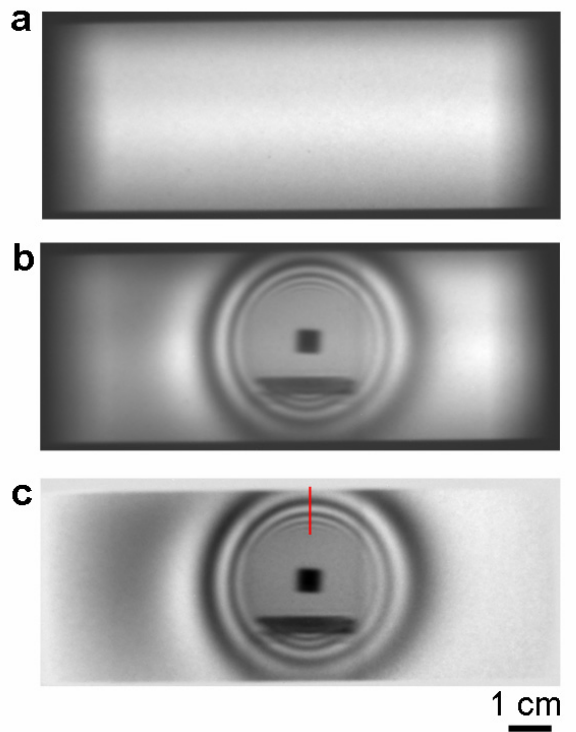


Fig. 5: A radiograph showing the field lines around a bar magnet levitating over an yttrium-barium-copper-oxide (YBCO) superconductor due to the Meissner effect. a) Flat field image without sample, b) radiograph as obtained by the experiment and c) flat field corrected image.

The transmission signal is a periodic function of the spin rotation angle ϕ (eq. 1) with alternating maximum and minimum transmission.

A cross section along the red line in Fig. 5 c) is shown in Fig. 6 in black. The curve has also been calculated taking into account a magnetic dipole field around the levitating magnet. Experiment and calculation are in good agreement. Slight deviations (left side fig. 6) are mainly caused by the finite wavelength of the neutron beam (causing a dephasing) and the limited spatial resolution.

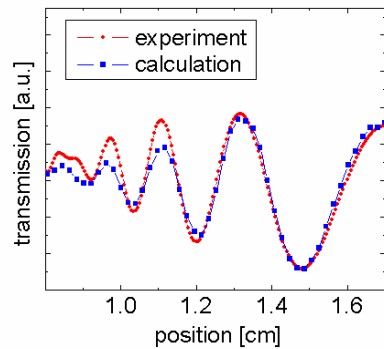


Fig. 6: Cross section along the red line in Fig. 5 c) (red) and corresponding calculated curve (blue) [11].

In the next example the current distribution in a conducting cylindrical aluminum rod with a diameter of 4 cm was investigated. Two electrical contacts were fixed to the rod at the top and bottom surfaces (see Fig. 7 bottom left). This setup produces a magnetic field which is perpendicular to the vertically oriented magnetic moment of the neutrons. The contacts were placed at different positions off the centre of the circular cross section in order to simulate a non-trivial case (see image bottom right in Fig. 7). A current of 25 A was applied. Images were taken at different frequencies with an exposure time of 120 sec for a single image.

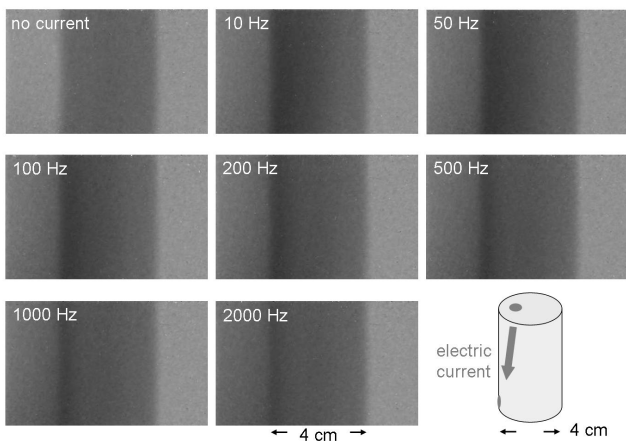


Fig. 7: Spin polarized neutron radiographs of a 4 cm thick aluminum rod without applied current and with 25 A alternating current at different current frequencies from 10 Hz to 2000 Hz. Due to the asymmetric electric contact and the skin effect the current is shifted to the left side at increased frequencies resulting in a corresponding shift of the magnetic field.

The first image (top right) in Fig. 7 shows a radiograph of the aluminum rod without an applied current. The image contrast is caused only by attenuation. The transmission of the polarization analyzer was at its maximum; i.e. no spin rotation occurred. Then an alternating current of 25 A at a frequency of 10 Hz was applied to the rod. This caused a current flow that was concentrated at the left side of the aluminum rod corresponding to the asymmetry of the electrical contact. A dark area can be identified at the left hand side in the corresponding neutron radiograph of Fig. 7. The magnetic field induced by the current causes a precession of the neutron spins around the field direction in this area and reduces the transmission signal.

Higher frequencies cause a current displacement to the edges of the rod due to the skin effect. In our case (for a cylindrical rod-shaped conductor) the so called skin depth δ marks the depth below the surface of the conductor at which the current density has fallen to $1/e$ of the value at the surface and can be calculated by

$$\delta = \sqrt{\frac{2\rho}{\omega\mu}}$$

where ω is the frequency of the applied alternating current, ρ is the resistivity of the conductor, and μ is the absolute magnetic permeability of the conductor.¹ Images taken at higher current frequencies up to 2000 Hz are shown in fig. 7. It can be clearly seen that the dark area shifts to the left side of the images. The current is displaced to the side and the dark area becomes narrower.

5. Conclusion

Since the presence and controlled application of magnetic fields are essential in many fields of science and technology as well as in fundamental physics, the presented method of polarised neutron imaging appears as a visualisation technique with a broad range of applications. As a radiographic method it is non-destructive and non-invasive and can be applied without any specific sample preparation (like garnet films). Polarised neutron imaging can help to address present day scientific challenges in fundamental magnetic research as well as in materials science and engineering.

References

- [1] P. Gammel and D. Bishop, Science 279(1998) 410
- [2] Ch. Jooss, J. Albrecht, H. Kuhn, S. Leonhardt and H. Kronmüller, Reports on Progress in Physics 65 (2002) 651
- [3] J. Banhart (ed), Advanced Tomographic Methods in Materials Research and Engineering, Oxford University Press (2008)
- [4] B. Schillinger, E. Lehmann, P. Vontobel, Physica B 276 (2000) 59
- [5] N. Kardjilov, A. Hilger, I. Manke, M. Strobl and J. Banhart, Nuclear Instruments and Methods A 542 (2005) 16
- [6] M.A. Hickner, N.P. Siegel, K.S. Chen, D.S. Hussey D.L. Jacobson and M. Arif, J. Electrochem. Soc., 155 (2008) B427
- [7] I. Manke, J. Banhart, A. Haibel, A. Rack, N. Kardjilov, A. Hilger, S. Zabler, A. Melzer, H. Riesemeier, Appl. Phys. Lett. 90 (2007) 214102
- [8] P. Boillat, D. Kramer, B.C. Seyfang, G. Frei, E. Lehmann, G.G. Scherer, A. Wokaun, Y. Ichikawa, Y. Tasaki and K. Shinohara, Electrochim. Comm. 10 (2008) 546
- [9] I. Manke, C. Hartnig, N. Kardjilov, M. Messerschmidt, A. Hilger, M. Strobl, W. Lehnert and J. Banhart, Appl. Phys. Lett. 90 (2007) 244101
- [10] I. Manke, C. Hartnig, N. Kardjilov, M. Grünerbel, A. Hilger, J. Kaczerowski et al, Appl. Phys. Lett. 90 (2007) 184101
- [11] N. Kardjilov, I. Manke, M. Strobl, A. Hilger, W. Treimer, M. Meissner, T. Krist and J. Banhart, Nature Physics 4 (2008) 399

- [12] M. Strobl, W. Treimer, P. Walter, S. Keil and I. Manke, *Appl. Phys. Lett.* 91 (2007) 254104
- [13] M. Hochhold, H. Leeb and G. Badurek, *Journal of Magnetism and Magnetic Materials* 157-158 (1996) 575
- [14] E. Jericha, R. Szeywerth, H. Leeb and G. Badurek, *Physica B* 397 (2007) 159
- [15] F. Mezei, *Zeitschrift für Physik* 255 (1972) 146
- [16] Th. Krist, S.J. Kennedy, T.J. Hick, F. Mezei, *Physica B* 241-243 (1998) 82